Superlattices and Microstructures 98 (2016) 242–252

Contents lists available at ScienceDirect

Superlattices and Microstructures

journal homepage: www.elsevier.com/locate/superlattices

Growth and characterization of nanocrystalline PbS:Li thin films

M. Chávez Portillo [a, *], X. Mathew [b], H. Juárez Santiesteban [a], M. Pacio Castillo [a], O. Portillo Moreno [c]

[a] Benemérita Universidad Autonoma de Puebla. CIDS, Av. San Claudio y 18 Sur, Col. San Manuel, Ciudad Universitaria, CP 72570, P.O. Box 1067, Puebla, Pue., 7200, Mexico
[b] Instituto de Energías Renovables, Universidad Nacional Autónoma de México, 62580 Temixco, Morelos, Mexico
[c] Benemérita Universidad Autónoma de Puebla Lab. de Ciencias de Materiales de la Facultad de Ciencias Químicas, P.O. Box 1067, Puebla, Pué., 72001 Mexico

ARTICLE INFO

Article history:
Received 16 August 2016
Accepted 19 August 2016
Available online 21 August 2016

Keywords:
PbS:Li
Nanocrystals
Urbach tail
Quantum confinement

ABSTRACT

The structural, electrical and opto-electronic properties of PbS thin films doped with Li^+ ion were investigated. The crystallite size showed a strong dependence on Li doping, the crystal size changed from 36 nm to 12 nm due to Li incorporation in PbS. Optical band gap showed a shift in the range ~1.5–2.3 eV with Li incorporation. Urbach tailing in the band gap was observed and the Urbach energy has a dependence on the amount of incorporated Li. SEM images showed a notable change in grain size with Li doping, however the morphology changes from large grains to agglomerations of smaller grains when doped with Li. The electric conductivity of the films showed a dependence on Li doping, reached a maximum value and later decreased for higher Li containing films. The doped samples showed better photosensitivity.

1. Introduction

The band gap of PbS can be tuned in the range 0.4–5.0 eV [1] via size control, which makes it a promising material for optoelectronic applications including telecommunications [2], LEDs [3], lasers [4], photodetectors [5], and photovoltaic devices [6–9]. Alkali metals are monovalent cations that can substitute Pb^{2+} supplying free carriers in the structure for application in solar cells [10]. PbS is a semiconductor material with a E_g of 0.4 eV in bulk, and relatively large exciton Bohr radius of 18 nm [11], which allows strong quantum confinement of both electrons and holes. The value of the E_g can be simply controlled by modifying the grain size (GS) and this is achieved by controlling systematically the deposition temperature and doping [12]. The absorption edge has been found to blue shifted significantly as particle size reduced. Also polycrystalline PbS thin films showed good photoconductive properties, these properties have been correlated with the synthesis method, thickness, composition and structure.

Various methods for the preparation of PbS nanocrystals have been reported such as SILAR [13], chemosynthesis [14], Chemical bath deposition (CBD) [10], etc. In the present report, PbS and PbS:Li films were prepared by CBD, which involves the immersion of a glass substrate in alkaline lead–thiourea yielding PbS films of 100–500 nm thickness. CBD method has

* Corresponding author.
E-mail address: melussa03@hotmail.com (M.C. Portillo).

http://dx.doi.org/10.1016/j.spmi.2016.08.032
0749-6036/

become an attractive technique for the growth of films due to several advantages compared to other techniques, including scalability to large area, low cost, ability to deposit thin films on different substrates, and flexibility of tuning thin film properties simply by controlling and adjusting the deposition parameters. In addition CBD allows easy incorporation and control of the dopants as well as the reproducibility of the samples. In the present work we are reporting CBD preparation of PbS:Li thin films, and the structural, morphological, electrical, optical, and opto-electronic properties of the deposited films as a function of Li^+ concentration. A systematic investigation of the CBD prepared PbS:Li will enhance the knowledge about the Li^+ incorporation in PbS and associated changes in grain size and quantum confinement effects.

2. Experimental

2.1. Chemical reactions and film deposition

Chemical reactions for the growth of doped and undoped PbS films were determined by employing the reported cell potential values in basic media. The cell potential and the Gibbs free energy are related through the Nernst equations: $\Delta G^\circ = -n\tau\varepsilon^\circ$ [10]. The slow process at the substrate surface take place predominantly over direct hydrolysis of thiourea in the bulk of the reaction bath as follows:

$$SC(NH_2)_2 + 3OH^- \Leftrightarrow CO_3^{2-} + S^{2-} + 7H^+ \quad (1)$$

$$[Pb(NH_3)_4]^{2+} + S^{2-} \Leftrightarrow PbS + 4NH_3$$

$$\Delta G^o = +362.88\ \text{KJ} \quad (2)$$

Li^+ ion is generated by the dissociation of Li(OH) according to

$$LiOH \Leftrightarrow Li^+ + OH^-$$

$$\Delta G^o = +140.08\text{KJ} \quad (3)$$

PbS doping is happened according to the following reaction

$$[Pb(NH_3)_4]^{2+} + S^{2-} + Li(OH) \Leftrightarrow PbSLi^+ + 4NH_3 + OH^-$$

$$\Delta G^o = +592.96\text{KJ} \quad (4)$$

Finally, according to the numerical value of $\Delta G^\circ > 0$, it is concluded that Li is incorporated in the PbS as Li^+ ion.

Experimental details for depositing PbS:Li films are similar to those reported in previous work [14,15]. The PbS bath contained $Pb(CH_3CO_3)_2$ (0.04M), KOH (0.2 M), NH_4NO_3 (1.3 M), and $SC(NH_2)_2$ (0.3 M). Thin films with eight different volume levels of Li doping ($V_{[Li]}$) were obtained by the addition in situ of 1–8 ml of $Li(NO_3)$(0.04M) to the above bath. The different batches of solutions were stirred well and kept at 40 ± 2 °C during 30 min. The adequate molarity of 0.04 of the doping solution was determined experimentally on the basis of film adherence. The samples were labelled as PbS for undoped film and PbS:Li1–PbS:Li8 for doped films, where the numbers 1–8 corresponds to the volume (ml) of $Li(NO_3)$ added to the PbS bath.

2.2. Material characterization

The structural characterization was carried out using the X-ray diffraction (XRD) patterns recorded on a Bruker D8 Discover Diffractometer, using the Cu K_α line. Morphological features were investigated using a Hitachi S5500 FESEM. The optical absorption spectra were recorded using a UV-Vis-NIR Varian 5000 Spectrophotometer, the photoresponse of the films were studied using a computerized homebuilt system.

3. Results and discussion

Fig. 1 shows the SEM images of two typical samples; (a) pure PbS, and (b) PbSLi6, which is the film deposited from the PbS bath containing 6 ml of $Li(NO_3)$(0.04M) as discussed in section 2.1. The effect of doping is very clear, grain size was significantly lowered and the film surface feature agglomeration of large numbers of smaller grains. Fig. 1(a) resembles the typical morphology of PbS obtained by CBD [16,17].

Fig. 2 (a) shows the X-ray diffractograms of pure PbS as well as the PbS:Li films. All the diffraction peaks corresponds to the PbS as reported previously [17]. According to reference pattern JCPDS 05–0592 the PbS crystallizes in the cubic (zinc-blende) phase.

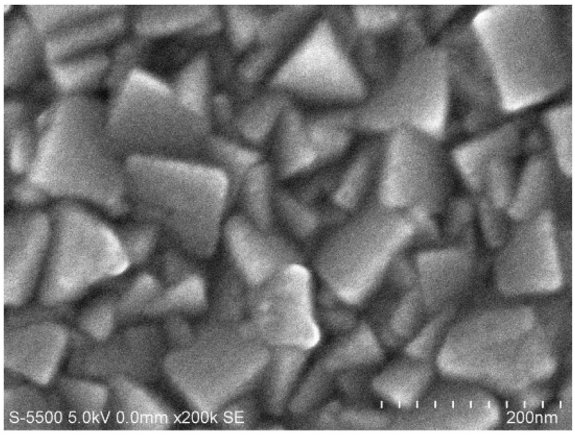

(a)

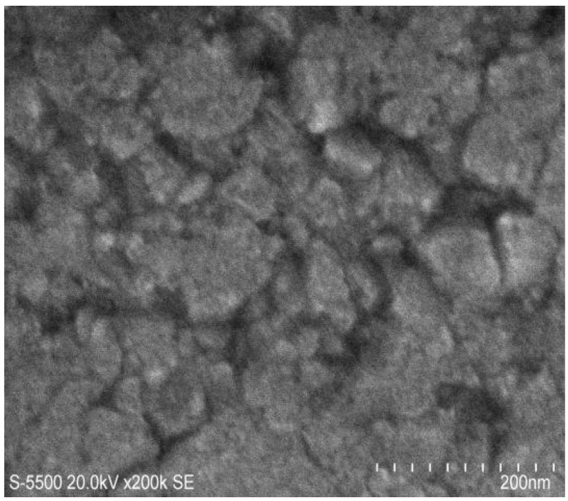

(b)

Fig. 1. SEM images of: (a) PbS, and (b) PbSLi6.

The three prominent effects observed in XRD patterns as a result of doping are the shift of diffraction bands, band broadening, and decrease in intensity. These effects are attributed to the formation of a solid solution [18,19]. The band broadening can be due to disorder in the crystals, e.g., due to strain and reduction in the grain size (GS). In order to stabilize the crystal structure the GS is reduced thereby releasing the strain. The inset of Fig. 2 (a) shows the GS vs. $V_{[Li]}$ plot for PbS:Li samples. The grain size decrease from ~35 nm (PbS) to ~12 nm (PbS:Li8), which is related to the incorporation of Li^+ ion in the crystal lattice. The shift of the (111) diffraction peak towards higher angles (Fig. 2(b)) with Li doping concentration indicates a decrease in inter-planar distance. A possible reason can be the ionic radius of Li^+ dopant; the ionic radii are $Pb^{+2} = 1.20$ Å, $S^{2-} = 1.84$ Å and $Li^+ = 0.73$ Å.

Fig. 3 shows the transmittance (T) spectra of the PbS, and PbS:Li films. A notable feature is the shift in absorption edge to lower wavenumbers as a result of the increase in doping concentration.

The optical absorption coefficient (α) vs. wavelength spectra of PbS and PbS:Li films are shown in Fig. 4 (a). Large blue-shift of the absorption onset with respect to the bulk PbS indicate the quantum confinement effect [20]. Zhao et al. also observed this behaviour for the synthetized PbS nanomaterial and speculated that the position-dependent quantum-size effects exist for relatively large faceted nanocrystals (stars and octahedrons) with regular shapes, resulting in dramatically blue-shifted excitonic absorptions [21]. PbS have the second excitonic manifold $^1P_h \rightarrow {}^1P_e$ at ~800 nm (1.4 eV) originating from the four equivalent *L* valleys in the Brillouin zone [22]. Fig. 4 (b) is a diagram depicting the transitions of the exciton peaks for PbS nanocrystals [23]. This excitonic peaks are related to the third, fourth, and fifth excitonic transitions corresponding to the $^1D_e \rightarrow {}^1D_h$, $^2S_e \rightarrow {}^2S_h$ and $^2P_e \rightarrow {}^2P_h$ transitions located at ~880, 750, 680, 570 nm [24]. The large Bohr radius of PbS (18 nm) contributes to the observed optical properties, similar transitions are rarely observed for semiconductors with smaller Bohr

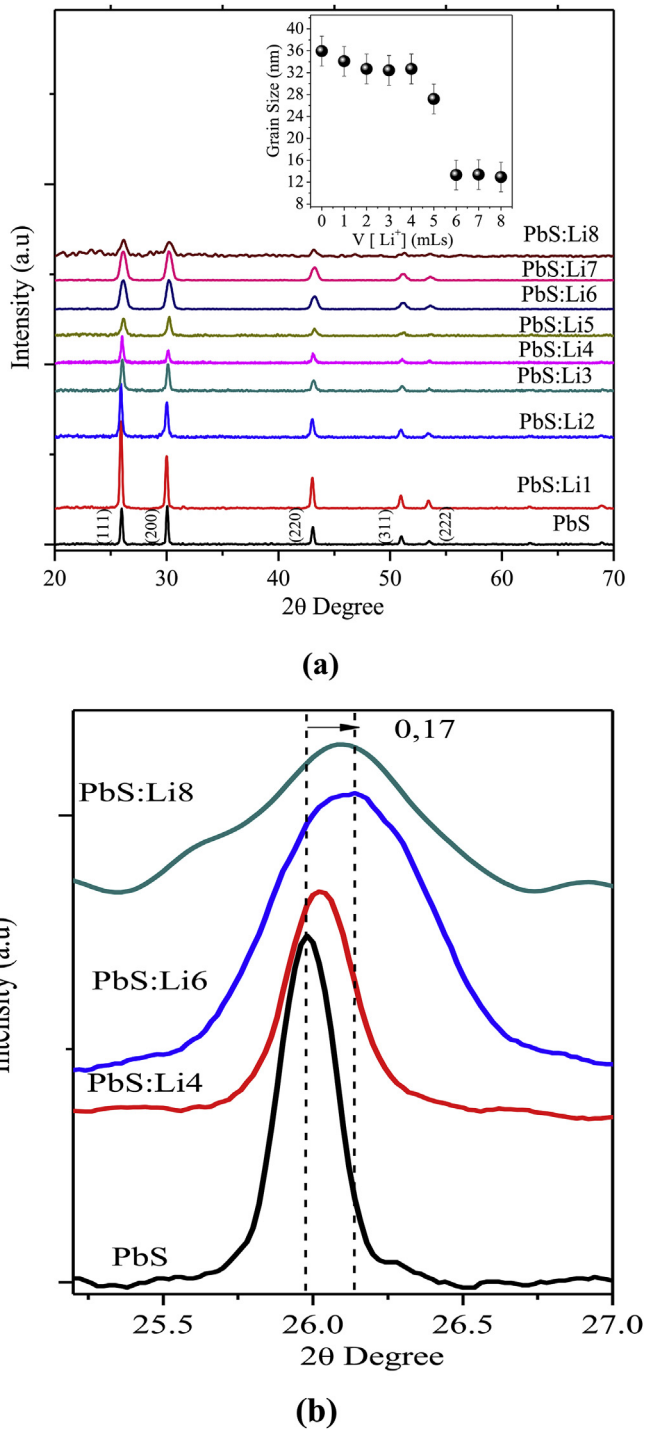

Fig. 2. (a) XRD patterns of PbS and PbS:Li samples, (b) shift of the reflection from (111) plane of PbS due to Li doping. Inset of Fig. 1a shows the variation of grain size with Li doping.

radius. It is also possible that these bands correspond to transitions into high-energy levels rather than excitonic transitions. Chalita et al. reported that depending on PbS particle size the absorption edges are located at ~529, ~760, ~1104, ~1497 nm when the PbS nanocrystals are of 2.4, 3.6, 5.6, 9.4 nm respectively [25]. The absorption edge clearly shows a blue shift in contrast to absorption region at ~3200 nm for PbS ($E_g = 0.42$ eV) [26].

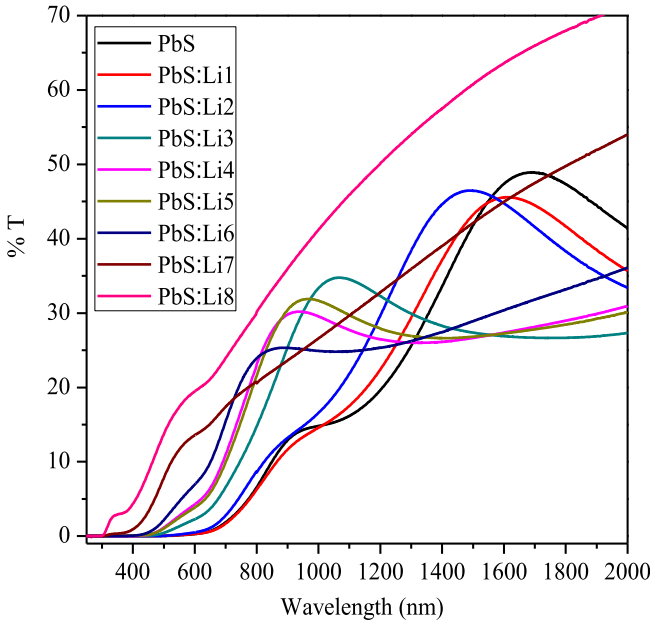

Fig. 3. Transmittance vs. wavelength plots of PbS and PbS:Li films.

The band gap (E_g) of all the films has been calculated with the help of absorption spectra and the Tauc's relation $(\alpha h\nu) = A(h\nu - E_g)^n$, where $h\nu$ is the photon energy, h is Planck's constant, α is the absorption coefficient, A is constant, and $n = 1/2$ for direct transitions. The usual method of determining E_g is to plot a graph $(\alpha h\nu)^2$ vs. $h\nu$ and determine the intercept of the straight-line fit at the energy axis [27]. Fig. 5 (a) show the $(\alpha h\nu)^2$ vs. $h\nu$ plot of PbS and PbS:Li films, and the obtained E_g values are plotted in Fig. 5(b) in relation to Li concentration in the bath. It is clear that the band gap shows a strong dependence on Li concentration which in turn related to a decrease in particle size. Thus, the observed large shift demonstrates the existence of quantum confinement effect in these films [28]. Similar excitonic effect was observed in CdSe nanocrystallites [29,30]. The range of E_g measured in our work indicate that the PbS films contain large as well as nanocrystalline particles [31]. Similar blue shift in E_g values for the films with smaller thickness or GS have been reported for chemically deposited metal chalcogenide films [32].

The α near the fundamental absorption edge shows an exponential dependence on the incident photon energy and obeys the empirical Urbach relation according to: $\alpha = \alpha_0[\exp(h\gamma/E_u)]$ [14], where α_0 is a constant and E_u is the Urbach energy, which characterizes the slope of the exponential region. The E_u absorption edge is formed in the region below band gap. Therefore, E_u gives the width of the localized states associated with nanocrystalline or amorphous structures in the band gap of the material. It is believed that the exponential dependence of α on $h\nu$ can be attributed to random fluctuations of the internal fields associated with the structural disorder in many nanocrystalline or amorphous materials [33]. Fig. 6(a) shows the $\ln(\alpha)$ vs. $h\nu$ plots for PbS:Li samples. From Fig. 6 (b) it is clear that the $V_{[Li]}$ has a notable influence on E_u, indicating different types of disorders in the absorption processes at the long wavelength side of the fundamental absorption edge. Based on these observations which are similar to that reported [34], it can be concluded that the decrease in E_u is related to the Li^+ ion incorporation and the reduction of the grain size, which in turn resulted in films with more order in the lattice and smaller density of localized states. The incorporation of foreign ions could introduce trap states at the surface and grain boundaries. Introduction of Li^+ ions increase carrier concentration which induce band tailing in the E_g and scattering due to electron-impurity interaction [35].

Fig. 7 shows the E_u vs. E_g plot for PbS:Li films. In this plot a decrease in E_u with E_g is seen which can be associated with the existence of stacking faults and grain boundaries. Similar behavior of E_u vs. E_g was reported and related to ionic radii of dopants [36].

The photocurrent characteristic of the PbS and PbS:Li samples were measured by utilizing two co-planar metallic contacts painted on the surface of the films. The current measurements were performed in dark and under light by applying a constant potential of 10 V. The measurement sequence was 20 s in dark, 10 s in light, and 20 s in dark after the illumination period. The I-t data of the different samples measured under identical conditions are shown in Fig. 8. It is clear that the conductivity increases with Li doping, attains a maximum and decreases (Fig. 9), and in general doped samples are more photosensitive. As can be seen in Fig. 9, the conductivity has a dependence on $V_{[Li]}$, PbS:Li5 and PbS:Li6 show higher conductivity. The decrease in conductivity for higher doping levels could be due to recombination and decrease in lifetime of charges carriers.

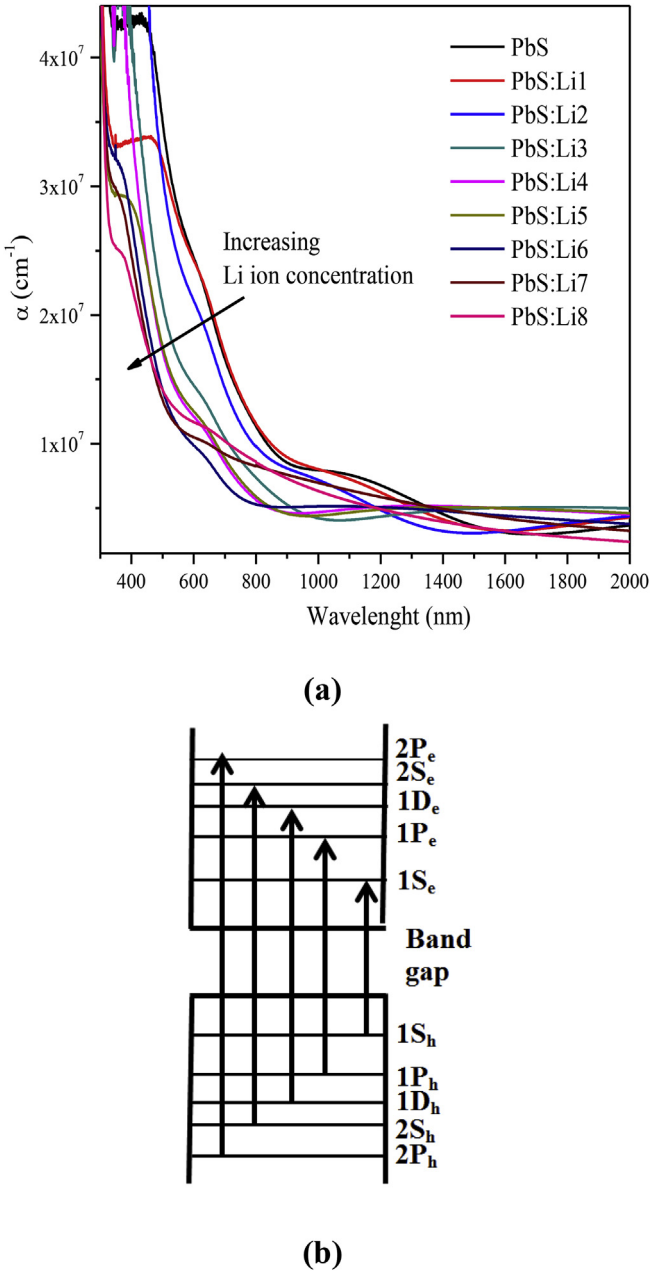

Fig. 4. (a) Optical absorption coefficient of the PbS and PbS:Li films, (b) schematic of the quantized energy levels of nanocrystals of PbS.

The photosensitivity of the samples was estimated using the following relation [37];

$$S = \frac{\sigma_L - \sigma_{dark}}{\sigma_{dark}}$$

where I_L and I_{dark} are the current in light and dark conditions respectively. The photosensivity of different samples as a function of $V_{[Li]}$ is shown in Fig. 10. There is no noticeable tendency for the photosensitivity with respect to the $V_{[Li]}$. The higher photosensitivity of PbS:Li8 is attributed to the high resistivity of the film. It can be mentioned that the Li doping made the films more photosensitive.

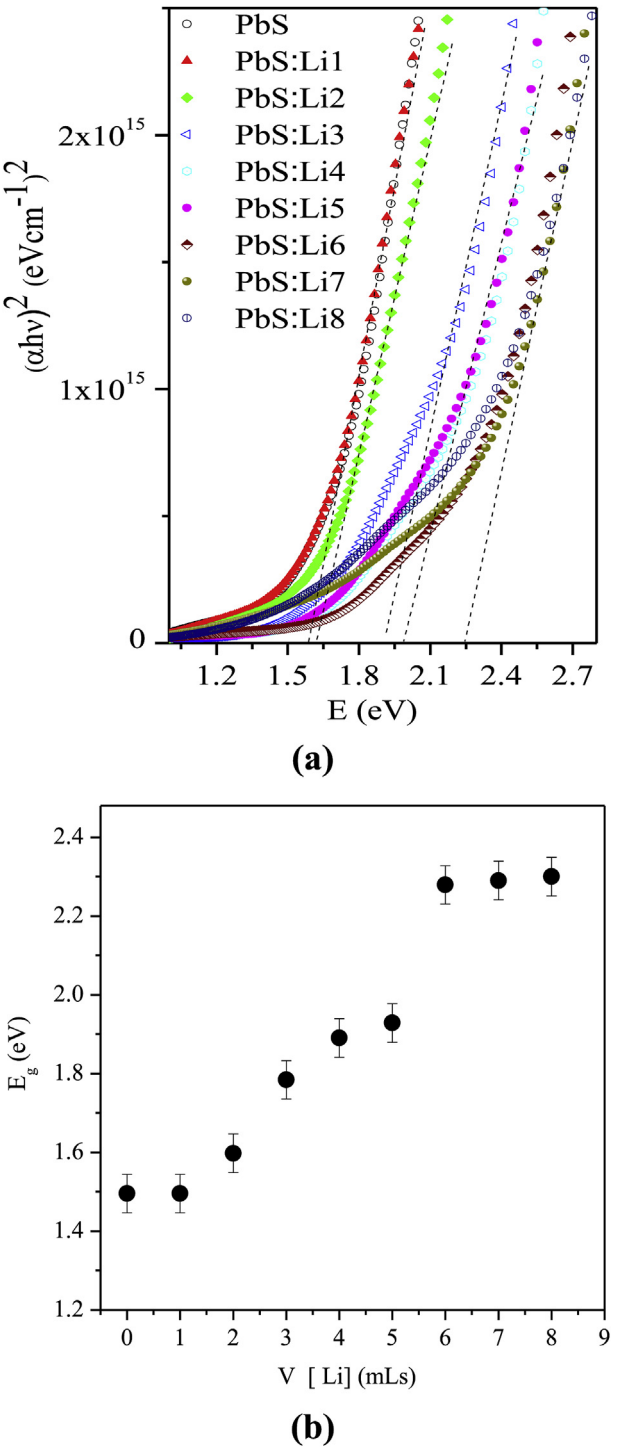

Fig. 5. (a) graph of $(\alpha h\nu)^2$ vs. hν, and (b) E_g vs. of $V_{[Li]}$ for the PbS:Li films.

4. Conclusions

In this work we have developed pristine PbS and PbS:Li films through a wet chemical route. The obtained films showed p-type conductivity, and a strong dependence for all material properties on the amount of Li incorporated in the PbS. The

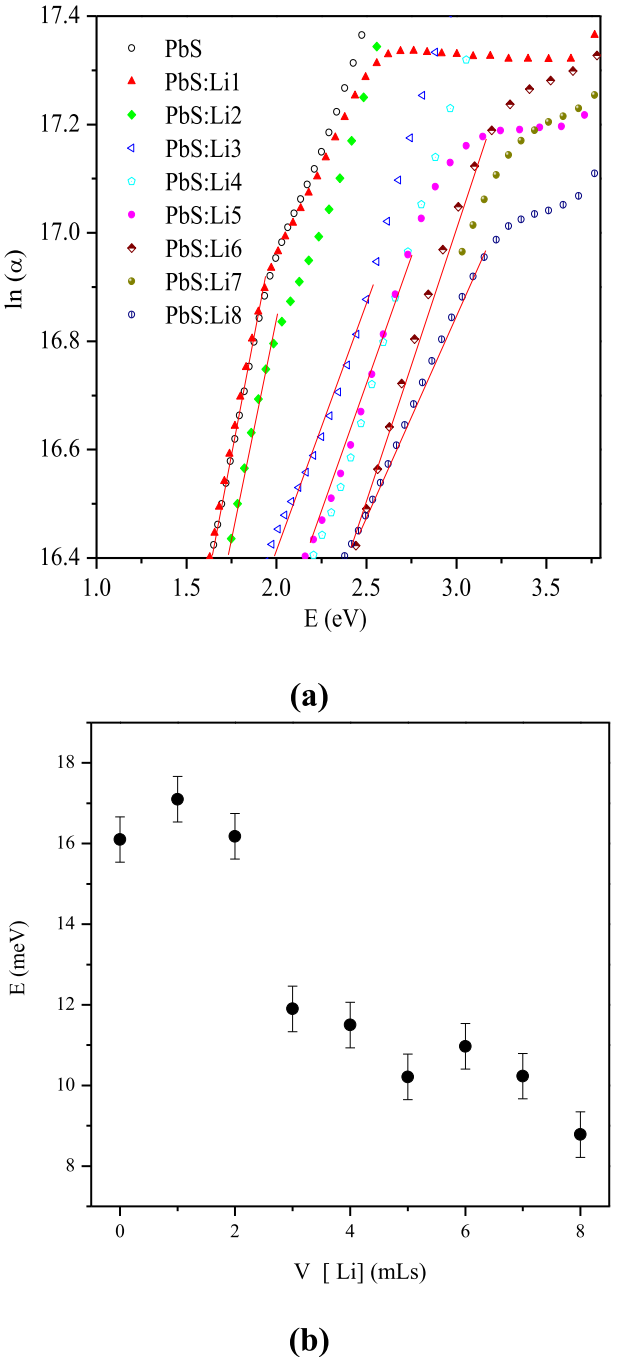

Fig. 6. (a) Plots of ln(α) vs. hv; (b) E_u vs. V [Li].

crystallite size changed from 36 nm of the pristine PbS to 12 nm for the Li doped film. The inter-planar distance of PbS decreased as a result of doping. The SEM images showed that the pristine PbS crystallizes with well-faceted large grains, however the morphology changes from large grains to agglomerations of smaller grains when doped with Li. Optical band gap was blue shifted from ~1.5 eV to 2.3 eV with Li incorporation, and Urbach tailing in the band gap was observed with a notable dependence on the amount of incorporated Li. The observed blue shift indicates possible quantum confinement in PbS:Li. The electric conductivity of the films showed a dependence on Li doping, reached a maximum value and later decreased for higher Li containing films. The doped samples showed better photosensitivity.

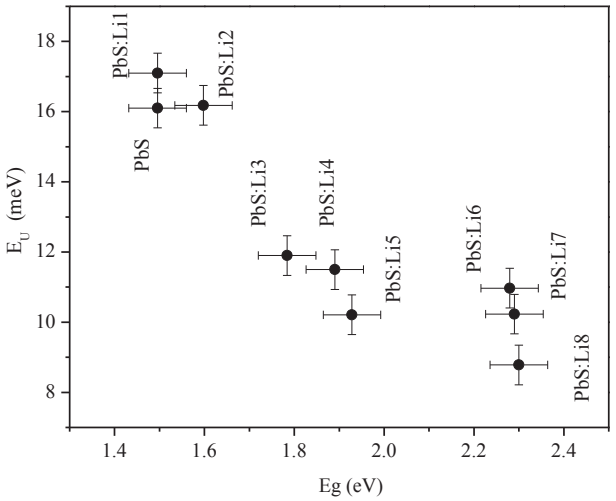

Fig. 7. E_u vs. E_g plot for PbS:Li films.

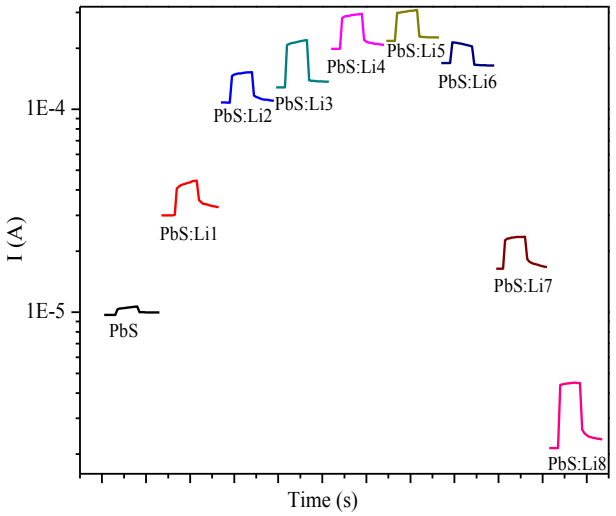

Fig. 8. Current vs. time response of PbS and PbS:Li samples, the illumination intensity was 100 mW/cm^{-2} from a tungsten-halogen lamp.

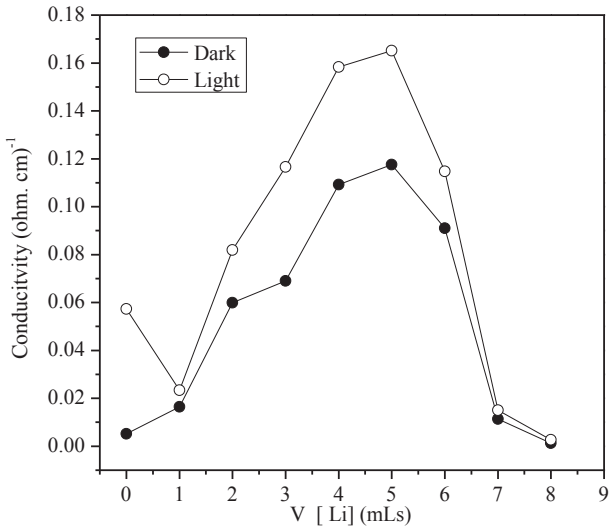

Fig. 9. Conductivity vs. $V_{[Li]}$ for the PbS and PbS:Li thin films.

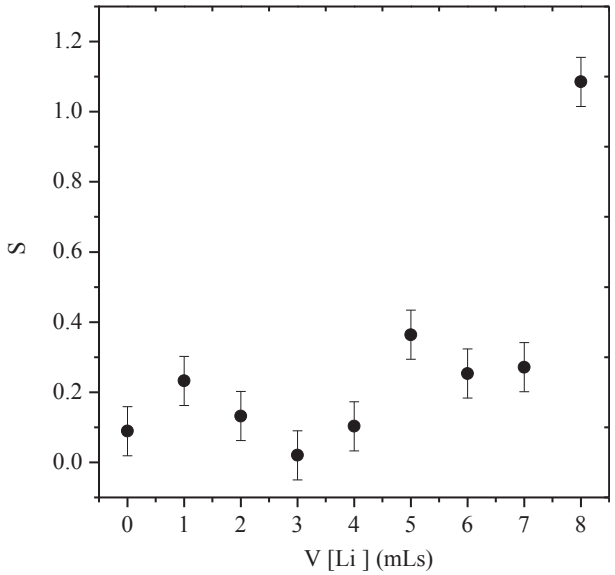

Fig. 10. Variation of photosensitivity of the PbS and PbS:Li films.

Conflict of interest

The authors have no conflicts of interest to declare.

Acknowledgements

Some of the material characterizations presented in this manuscript is supported by the projects CeMIE-Sol PY-207450/ P25, P26 and P28, with the intention to study this material as possible back contact layers to the devices under development in those projects.

References

[1] R. Thielsch, T. Bohne, R. Reiche, D. Schlafer, H.D. Bauer, H. Bottcher, Quantum- size effects of PbS nanocrystallites in evaporated composite films, Nanostruct. Mater. 10 (1998) 131.
[2] J.S. Steckel, S. Coe-Sullivan, V. Bulovic, M.G. Bawendi, 1.3 μm to 1.55 μm tunable electroluminescence from PbSe quantum dots embedded within an organic device, Adv. Mater. 15 (2003) 1862.
[3] A.L. Rogach, N. Gaponik, J.M. Lupton, C. Bertoni, D. Gallardo, D. Dunn, N. Pira, M. Paderi, P. Reppeto, S. Romanov, C.O.' Dwyer, C. Sotomayo, A. Eychmuller, Light emitting diodes with semiconductor nanocrystals, Angew. Chem. Int. Edn. 47 (2008) 6538.
[4] H. Eisler, V.C. Sundar, M.G. Bawendi, M. Walsh, H.L. Smith, V. Klimov, Color selective semiconductor nanocrystal laser, Appl. Phys. Lett. 80 (2002) 4614.
[5] G. Konstantatos, I. Howard, A. Fischer, S. Hoogland, J. Clifford, E. Klem, L. Levina, E.H. Sargent, Ultrasensitive solution cast quantum dot photodetectors, Nature 442 (2006) 180.
[6] S. McDOnald, G. Konstantatos, Shiguo Zhang, P. Cyr, E. Klem, L. Levina, H. Sargent, Ultrasensitive solution-cast quantum dot photodetectors, Nat. Mater. 4 (2005) 138.
[7] X. Jiang, R.D. Schaller, S.B. Lee, J.M. Pietryga, V.I. Klimov, Anvar A. Zakhidov, PbSe nanocrystal/conducting polymer solar cells with an infrared response to 2 micron, Mater. Res. 22 (2007) 2204.
[8] A.S. Obaid, M.A. Mahadi, Z. Hassan, Nanocoral PbS thin film growth by solid- vapor deposition, Optoelectron. Adv. Materials-Raid Commun. 6 (2012) 422–426.
[9] A. Stavrinadis, A. Rath, F. Pelayo, S.I. Diedenhofen, C. Magen, L. Martinez, D. So, G. Konstantatod, Heterovalent cation substitutional doping for quantum dot homojunction solar cell, Nat. Commun. 4 (2013) 2981.
[10] Z. Quan, C. Li, X. Zhang, J. Yang, C. Zhang, J. Lin, Polyol-mediated synthesis of PbS crystal: Shape evolution and growth mechanism, Cryst. Growth Design (2008) 72384–73492.
[11] R. Palomino Merino, O. Portillo Moreno, J.C. Flores Gracia, J. Hernandez Tecorralco, J. Martinez Juarez, A. Moran Torres, E. Rubio Rosas, G. Hrenandez Tellez, R. Gutierrez, L.A. Chaltel Lima, J. Nanoci. Nanotech. 14 (2014) 5408–5414.
[12] A.G. Kontos, Vlassis Likodimos, E. Vassalou, I. Kapogianni, Y.S. Raptis, Costas Raptis, P. Falaras, Nanostructured titania films sintetized by quantum dot chalcogenides, Nanoscale Res. Lett. 6 (2011) 266–272.
[13] S.B. Pawara, J.S. Shaikh, R.S. Devan, Y.R. Ma, D. Haranath, P.N. Bhosale, P.S. Patil, Facile and low cost chemosynthesis of nanostructured PbS with tunable optical properties, Appl. Surf. Sci. 258 (2011) 1869–1875.
[14] M. Chavez, H. Juarez, M. Pacio, X. Mathew, R. Gutierrez, M. Zamora, O. Portillo, Optical band gap energy and Urbach tail CdS: Pb2+ thin films, Rev. Mex. Física 62 (2016) 124–128.
[15] R. Palomino Merino, O. Portillo Moreno, L.A. Chaltel Lima, R. Gutierrez Perez, M. De Icaza Herrera, V. Castaño, Chemical deposition of PbS: Hg2+ nanocrystalline thin films, J. Nanomater. (2013) 6.
[16] B. Altioka, M. Celattin, M. Riza, Some physical effects of reaction reaction rate rate on PbS thin films obtained by chemical bath deposition, J. Cryst. Growth 384 (2013) 6.

[17] R.K. Joshi, A. Kanjilaland, H.K. Sehgal, Size dependence of optical properties in solution-grown $Pb_{1-x}Fe_xS$ nanoparticle films, Nanotechnology 14 (2003) 809–812.
[18] M. Chavez Portillo, M. Pacio Castillo, H. Juarez Santiesteban, Structural, optical and electrical characterization of Li doped PbS thin films, J. Mater. Sci. Eng. (2015), http://dx.doi.org/10.4172/2169-0022.C1.035.
[19] A. Bachmaier, M. Kerber, D. Setman, R. Pippa, The formation of supersaturated solid solutions in Fe–Cu, Acta Mater. 60 (2012) 860–871.
[20] C. Liu, Y. Kon Kwon, J. Heo, Absorption and photoluminescence of PbS QDs in glasses, J. Non-Crystalline Solids 355 (2009) 1880–1883.
[21] N.N. Zhao, L.M. Qi, Low-temperature synthesis of Star-shaped PbS nanocrystals in aqueous solutions of mixed cationic/anionic Surfactants, Adv. Mater. 18 (2006) 359.
[22] J.M. An, A. Franceschetti, A. Zunger, The Excitonic exchange splitting and radiative lifetime in PbSe Quantum dots, Nano Lett. 7 (2007) 2129–2135.
[23] F. Yoshino, A.A. Major, L. Levina, E.M. Sargent, Nonlinear refractive properties in lead sulfide (PbS) nanocrystals from 1200 to 1550 nm, in: Quantum Electronics Conference, 2004. (IQEC). International, San Francisco, CA, 2004, pp. 527–529.
[24] J. Zhang, X. jiang, Steady state photoinduced absortion of PbS quantum dots film, Appl. Phys. Lett. 92 (2008) 141108.
[25] C. Ratanatawanate, C. Xiong, Kennet J. Balkus Jr., Fabrication of PbS quantum dot doped TiO_2, Nanotub. Acsnano 8 (2008) 1682–1688.
[26] F.W. Wise, Lead salt quantum dots: the limit of strong quantum confinement, Acc. Chem. Res. 33 (2000) 773–780.
[27] S. Singhal, A. Kumar Chawla, H. Om Gupta, R. Chandra, Influence of Cobalt doping on the physical properties of $Zn_{0.9}Cd_{0.1}S$ nanoparticles, Nanoscale Res. Lett. 5 (2010) 323–331.
[28] Mat. Sci.. in Semicond. Process., 15 (2012)564–571. R. Kumar, R. Das, Mukul Gupta, V. Ganesan, Preparation of nanocrystalline Sb doped PbS thin films and their structural, optical and electrical characterization, Superlattices and Microstructures, 75 (2014), 601-612.
[29] A. Rivera Márquez, M. Rubín Falfán, R. Lozada Morales, O. Portillo Moreno, O. Zelaya Ángel, J. Luyo Alvarado, S. Meléndez Lira, L. Baños, Quantum confinement and crystalline structure of CdSe nanocrystalline films, Phys. Solid State 188 (2001) 1059.
[30] S.A. Al Kuhaimi, Influence of preparation technique on the structural, optical and electrical properties of polycrystalline CdS films, Vacuum 51 (1998) 349.
[31] F. Wahab, Gustavo E. Fernandez, J. Ho Kim, S. Jung, K. Kim, M. Hassan Sayyad, Jimmy Xu1, High Seebeck coefficient in solution-grown PbSFilms, J. Electron. Mater. 43 (2014) 348–352.
[32] J.B. Biswal, N.V. Sawant, S.S. Garje, Deposition of rod- shaped antimony sulfide thin films from single source antimony thiosemicarbazone precursors, Thin Solid Films 518 (2010) 3164–3168.
[33] F. Yakuphanoglu, M. Arslan, The fundamental absortion edege and optical constants of some charge transfer compounds, Opt. Mater. 34 (2011) 265–268.
[34] P. Petrova, Urbach rule of $Bi_4Ge_3O_{12}$ doped with 3d and 4d ions, Opt. Mater. 34 (2011) 265–268.
[35] R. Vettumperumal, S. Kalyanaraman, B. Santoshkumar, R. Thangavel, Estimation of electron-phonon coupling and Urbach energy in Group-I elements doped ZnO nanoparticles and thin films by Sol-Gel method, Mater. Res. Bull. 77 (2016) 101–110.
[36] S.J. Ikhmayies, R.N. Ahmad-Bitar, A study of the optical bandgap energy and Urbach tail of spray-deposited CdS: in thin films, J. Mater. Res. Technol. 2 (2013) 221–227.
[37] P.J. George, A. Sanchez-Juarez, P.K. Nair, Modification of electrical, optical and crystalline properties of chemically deposited CdS films by thermal diffusion of indium and tin, Semicond. Sci. Technol. 11 (1996) 1090.